Magnetically induced phonon splitting in ACr_2O_4 spinels from first principles

Aleksander L. Wysocki
Ames Laboratory, U.S. Department of Energy, Ames, Iowa 50011, USA

Turan Birol
Department of Physics and Astronomy, Rutgers University, Piscataway, New Jersey 08854, USA
(Received 4 August 2015; revised manuscript received 23 March 2016; published 22 April 2016)

We study the magnetically-induced phonon splitting in cubic ACr_2O_4 (A = Mg, Zn, Cd) spinels from first principles and demonstrate that the sign of the splitting, which is experimentally observed to be opposite in $CdCr_2O_4$ compared to $ZnCr_2O_4$ and $MgCr_2O_4$, is determined solely by the particular magnetic ordering pattern observed in these compounds. We further show that this interaction between magnetism and phonon frequencies can be fully described by the previously proposed spin-phonon coupling model [C. J. Fennie and K. M. Rabe, Phys. Rev. Lett. **96**, 205505 (2006)] that includes only the nearest neighbor exchange. Using this model with materials specific parameters calculated from first principles, we provide additional insights into the physics of spin-phonon coupling in this intriguing family of compounds.

DOI: 10.1103/PhysRevB.93.134425

I. INTRODUCTION

The interplay of spin and lattice degrees of freedom can lead to a variety of fundamentally and technologically interesting phenomena including the spin-Jahn-Teller effect in frustrated magnets [1,2], magnetocapacitance [3], and the linear magnetoelectric effect [4,5]. One signature of this interplay is the influence of magnetic order on the vibrational spectrum of a material. In many transition metal oxides the spin correlations shift the phonon frequencies, and lead to the so-called magnetodielectric effect [6,7]. Furthermore, if the long-range antiferromagnetic (AFM) order reduces the crystal symmetry, the onset of antiferromagnetism can result in a substantial splitting of phonon frequencies that are degenerate in the paramagnetic (PM) phase, even when the change in the crystal structure is undetectable [8–12]. This phonon anisotropy is a nonrelativistic effect which originates from the changes in hybridization due to spin ordering. In particular, the phonon splitting can be phenomenologically explained by a dependence of the exchange interactions on the atomic positions [13,14].

Chromium spinels ACr_2O_4 (A = Mg, Zn, Cd) are a particularly interesting class of frustrated antiferromagnets that exhibit strong spin-phonon coupling. In the PM phase, group theory predicts, and experiments confirm, the presence of four triply degenerate infrared (IR)-active phonon modes. Below the Néel temperature, however, one of these phonon modes undergoes a large splitting into a singlet and a doublet [10,15–17]. This feature and its magnitude was argued to be a consequence of a dominant role of the nearest-neighbor (nn) direct Cr-Cr exchange interaction [10]. Fennie and Rabe [11] developed a general approach to incorporate material specific information from first principles into spin-phonon coupling models. They demonstrated that the spin-phonon coupling model with only nearest-neighbor exchange interaction and parameters derived from first principles provide a full description of experimentally observed magnetically-induced phonon splitting in $ZnCr_2O_4$ [11]. This model has later been successfully applied to many other systems as well [18–21].

Magnetically-induced phonon splitting have also been observed in other Cr-based spinels including $MgCr_2O_4$ and $CdCr_2O_4$. Interestingly, the sign of the phonon slipping observed for $MgCr_2O_4$ and $ZnCr_2O_4$ ($\omega_{\text{singlet}} > \omega_{\text{doublet}}$) [10,17] is opposite to that observed in $CdCr_2O_4$ ($\omega_{\text{doublet}} > \omega_{\text{singlet}}$) [15,16]. In all three of these compounds, the sign of the nn exchange interaction is the same, however its magnitude compared to further neighbor exchanges is dramatically different. In the Mg and Zn compounds the nn exchange interactions are two orders of magnitude larger than all other exchange interactions, while in $CdCr_2O_4$ the nn interaction is the same order as the second neighbor interaction. Based on this fact Kant *et al.* [17] concluded that the spin-phonon coupling model with only nn exchange interaction cannot explain the magnetically induced phonon anisotropy in ACr_2O_4 spinels and instead proposed that the phonon splitting is generally controlled by a nondominant, next nearest neighbor exchange interaction.

In this paper we use first principles calculations to study the magnetically induced phonon anisotropy of the zone-center polar modes in ACr_2O_4 (A = Mg, Zn, Cd) spinels. We show that the different magnetic orderings characteristic for these spinels lead to different signs of the phonon splitting. In particular, we explain the opposite sign observed for $ZnCr_2O_4$ and $MgCr_2O_4$ compared with $CdCr_2O_4$ which have distinct magnetic ground states. We find that the spin-phonon coupling model of Ref. [11] with only the nn exchange interactions can very accurately describe *ab initio* values of phonon frequencies for all the spinel compounds we considered.

II. METHODS

The first principles calculations were performed using the density functional theory (DFT) within the rotationally invariant DFT+U method [22] and the PBEsol approximation to the exchange-correlation functional [23]. Similarly as in Ref. [11] we used $U = 3$ eV and $J = 0.9$ eV, the parameters that accurately reproduce photoemission spectra and band gaps in sulfur Cr spinels [24].

The Kohn-Sham equations were solved using the projector augmented wave method [25] as implemented in the VASP code [26,27] (version 5.2). The valence basis included $3s$ and $3p$ states on Mg, $3d$ and $4s$ on Zn, $4d$ and $5s$ states on Cd, $5d$ and $6s$ on Hg, $3d$ and $4s$ on Cr, and $2s$ and $2p$ on O. The cutoff energies for the plane wave and augmentation charge were 500 eV and 605 eV, respectively. For the primitive unit cell of the cubic structure (two formula units) we used $6 \times 6 \times 6$ Γ-centered k-point mesh. For larger cells the k-point mesh was scaled accordingly (e.g., in order to accommodate the AFM-II order the primitive unit cell was enlarged by a factor of two along first two lattice directions and the $3 \times 3 \times 6$ k-point mesh was used). We checked that the calculated phonon frequencies are converged with respect to the k-point grid, see the Supplemental Material [28]. For density of states calculations $12 \times 12 \times 12$ k-point mesh (primitive unit cell of the cubic structure) was used. The self-consistent calculations were stopped when energy was converged down to 10^{-6} eV. The spin-orbit coupling was neglected in the calculations.

Structural relaxations were performed in the ferromagnetic (FM) state that preserves the cubic symmetry. The lattice parameter was manually varied and the energy was fitted to the parabola. For each value of the lattice parameter the ionic positions were relaxed until the Hellmann-Feynman forces were converged to less than 0.005 eV/Å. Phonon frequencies and eigendisplacements were calculated using the frozen phonons method using symmetry adapted modes obtained from the ISOTROPY package [29].

III. CRYSTAL AND MAGNETIC STRUCTURE

At high temperatures ACr_2O_4 spinels have a cubic ($Fd\bar{3}m$) structure where A^{2+} ions are in tetrahedral oxygen environment and form the diamond lattice, while Cr^{3+} ions are surrounded by octahedral oxygen cages and form a pyrochlore lattice, see Fig. 1(a). The calculated structural parameters are shown in the Supplemental Material [28].

The octahedral crystal field splits the Cr$3d$ orbitals into a lower-lying t_{2g} triplet and a higher-energy e_g doublet. Cr^{3+} has three outer electrons that fill the majority t_{2g} states which results in a net Cr spin $S = 3/2$. These features are illustrated in Fig. 2 where the spin resolved Cr $3d$ density of states (DOS) for $ZnCr_2O_4$ is shown.

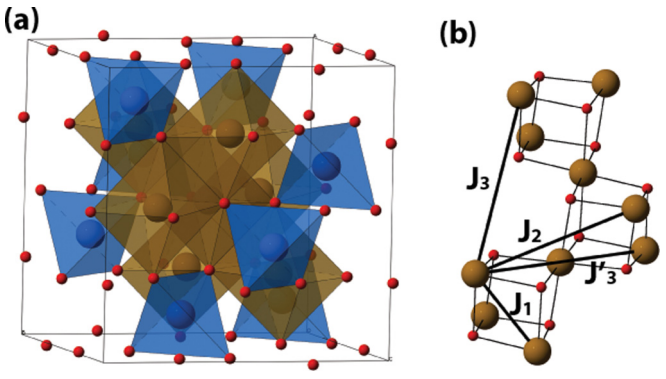

FIG. 1. (a) Cubic crystal structure of ACr_2O_4 spinels consisting of Cr-centered octahedra and A-centered tetrahedra. (b) Magnetic exchange couplings up to the third Cr neighbors; note that there are two nonequivalent types of third neighbors which have distinct exchange parameters: J_3 and J_3'. Brown, blue and red spheres denote Cr, A and O atoms, respectively.

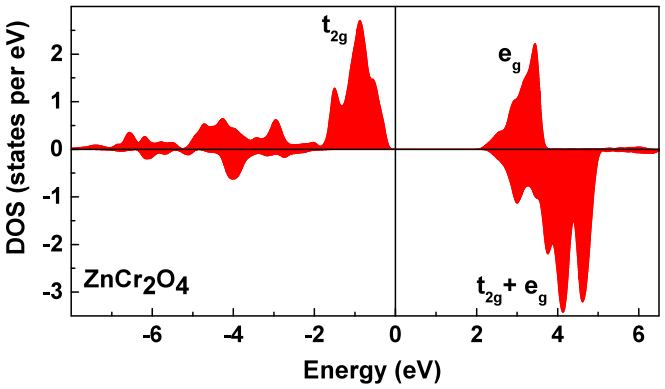

FIG. 2. Spin resolved Cr $3d$ DOS for $ZnCr_2O_4$ in the ferromagnetic state. Majority and minority DOS are plotted on positive and negative y axis, respectively.

We found the exchange interaction parameters between Cr spins by fitting *ab initio* energies of different collinear magnetic configurations to the Heisenberg Hamiltonian

$$H = \sum_{ij} J_{ij} \mathbf{S}_i \cdot \mathbf{S}_j \qquad (1)$$

where the summation is over Cr ions, $\mathbf{S}_i$ is the unit vector indicating the direction of the spin at Cr site i, and J_{ij} are the exchange parameters between Cr sites i and j. Positive (negative) exchange parameter indicate AFM (FM) coupling. We considered J_{ij} up to the third neighbors [Fig. 1(b)] as further neighbors are known to have negligible exchange couplings [30]. Exchange parameters for nn and next nn are denoted by J_1 and J_2, respectively. Since there are two nonequivalent types of third neighbors, we have two distinct third neighbors exchange parameters: J_3 and J_3'. The calculated exchange parameters are presented in Table I. Note that we also included the calculations for the $HgCr_2O_4$ compound.

The nn exchange parameter J_1 is a dominant interaction for all compounds. This coupling arises from the competition between AFM direct exchange and FM 90° superexchange [31]. For A^{2+} ions with small ionic radii, like Mg^{2+} or Zn^{2+}, the direct exchange mechanism dominates resulting in a strong AFM J_1. However, for larger A^{2+} ions the lattice parameter and the nn Cr-Cr distance increases [28], which diminishes

TABLE I. The exchange parameters (in meV) and $\mathcal{J}_{\lambda\perp,\parallel}/\omega_\lambda^{\mathrm{PM}}$ parameters (in cm^{-1}) calculated for different ACr_2O_4 spinels. Positive (negative) exchange parameter indicate AFM (FM) coupling.

A	J_1	J_2	J_3	J_3'	$\mathcal{J}_{\lambda\perp}/\omega_\lambda^{\mathrm{PM}}$				$\mathcal{J}_{\lambda\parallel}/\omega_\lambda^{\mathrm{PM}}$			
					1	2	3	4	1	2	3	4
Mg	3.8	−0.1	0.1	0.2	4.5	2.4	0.4	0.3	−0.1	−0.1	−0.7	−0.7
Zn	3.8	−0.1	0.1	0.2	2.0	5.0	0.8	0.2	−0.0	−0.1	−0.8	−0.7
Cd	0.3	−0.1	0.1	0.2	1.3	3.3	0.7	0.7	−0.0	−0.0	−0.5	−0.2
Hg	−0.6	−0.0	0.2	0.1	0.8	3.2	0.9	0.6	−0.0	−0.0	−0.5	−0.1

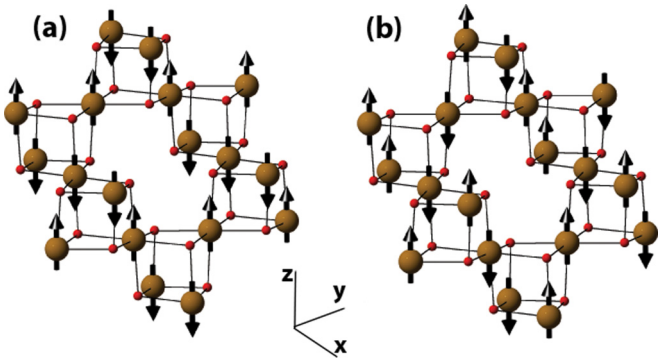

FIG. 3. Two collinear magnetic orderings relevant for ACr_2O_4 spinels. (a) AFM-I order that is similar to the true magnetic ground state in $ZnCr_2O_4$ and $MgCr_2O_4$. (b) AFM-II order that approximates the spin order in $CdCr_2O_4$. Brown and red spheres denote Cr and O atoms, respectively.

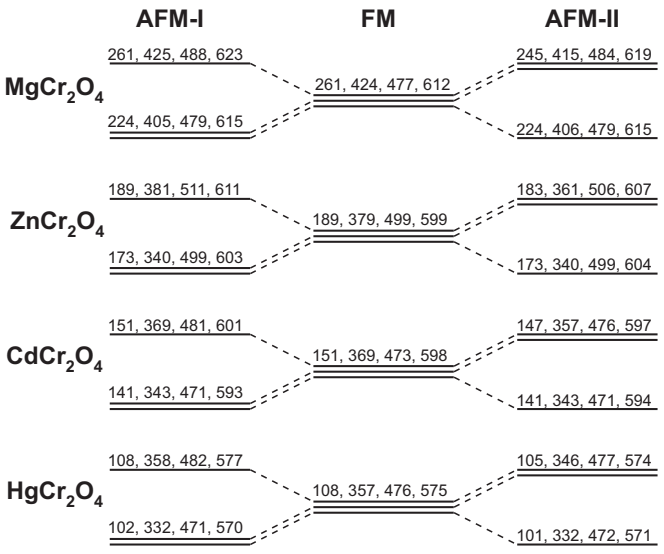

FIG. 4. Calculated T_{1u} phonon frequencies (in cm^{-1}) of different ACr_2O_4 spinels for different magnetic orderings. In the FM state (middle) there are four optical T_{1u} modes and each one is threefold degenerate. In the AFM-I (left) and AFM-II (right) states each triplet splits into a singlet and a doublet. For the AFM-I (AFM-II) ordering the singlet (doublet) has higher frequency for all compounds and for all phonon modes.

the direct exchange contribution. In particular, for $CdCr_2O_4$ the AFM J_1 is reduced by an order of magnitude while for $HgCr_2O_4$ the superexchange contribution overcomes the direct exchange resulting in a (small) FM J_1.

Exchange couplings beyond nn originate from higher-order superexchange processes [32] and, in general, are smaller than J_1. However, while for $MgCr_2O_4$ and $ZnCr_2O_4$ these interactions are negligible compared to the nn exchange, for $CdCr_2O_4$ and $HgCr_2O_4$ compounds the J_3 and J_3' exchanges become relevant.

The AFM nn exchange interaction is frustrated on the pyrochlore lattice since spins forming a tetrahedron cannot be all antiparallel to each other. The energy due to J_1 is minimized when for all tetrahedra the total spin is zero, i.e. in each tetrahedron two spins are parallel while the other two point in the opposite direction. There are, however, many such two-up-two-down configurations which can be different in different tetrahedra leading to infinite degeneracy. Consequently, the magnetic ground state is determined by further exchange couplings [33], magnetoelastic effects [1,2], or relativistic interactions [34] leading to complicated, often noncollinear (as in the case of $ZnCr_2O_4$ and $CdCr_2O_4$), orderings.

There are two primary collinear magnetic orders that are relevant for ACr_2O_4 spinels. These are shown in Fig. 3 and we denote them as AFM-I and AFM-II. The AFM-I ordering is similar to the true magnetic ground state in $ZnCr_2O_4$ [2] and $MgCr_2O_4$ [35] while the AFM-II approximates the spin order in $CdCr_2O_4$ [33]. Both spin orderings satisfy the two-up-two-down rule in each tetrahedron but they differ in relative orientations of spins in neighboring tetrahedra. In particular, for AFM-I the nearest neighbors in the xy plane are parallel while for AFM-II they are antiparallel. As we will see below, this difference has a profound effect on the magnetically induced phonon anisotropy. In the case of $HgCr_2O_4$ the magnetic ground state [36] cannot be approximated by neither AFM-I nor AFM-II orderings. Nevertheless, we found it beneficial to calculate the phonons for $HgCr_2O_4$ in AFM-I or AMF-II states since this allows us to assess the effect of the sign of the nn exchange parameter on the magnetically induced phonon anisotropy.

IV. PHONON FREQUENCIES

We now focus on the influence of magnetic order on the zone-center polar phonons. In addition to the AFM-I and AFM-II orderings which are relevant for this class of compounds (see above), we also considered the FM order since which has the same cubic symmetry as the PM state.

In the FM state there are four triply degenerate polar phonon modes, each transforming according to the T_{1u} irreducible representation of the O_h cubic point group. In order to compute the corresponding phonon frequencies we considered symmetry-adapted T_{1u} modes, $f_{n,\alpha}$. Here $n = 1,2,3,4,5$ is the mode number (in addition to four polar modes we need to include the acoustic mode that also has a T_{1u} symmetry) and $\alpha = x,y,z$ labels the row of T_{1u} such that $f_{n,\alpha}$ transforms as a vector along the α axis. The symmetry-adapted modes, $f_{1,\alpha}$, $f_{2,\alpha}$, and $f_{4,\alpha}$, involve atomic displacements along α of the entire A, Cr, and O sublattice, respectively. On the other hand, atomic displacements associated with $f_{3,\alpha}$ and $f_{5,\alpha}$ take place in the plane perpendicular to the α axis and involve chromium and oxygen atoms, respectively (see the Supplemental Material for more details).

Condensing the symmetry-adapted modes for a given α and evaluating the Hellman-Feynman forces for the FM state, we constructed the 5×5 dynamical matrix block. Matrix diagonalization leads then to four nonzero phonon frequencies corresponding to the four polar phonon modes, see Fig. 4 (middle). As expected, the frequencies are independent of α leading to threefold degeneracy of each mode.

For the AFM-I and AFM-II orderings the symmetry is lowered to tetragonal D_{4h} and D_4 point groups, respectively, with the tetragonal direction chosen to be along the z axis. In both cases the T_{1u} representation becomes reducible resulting

in a splitting of the triple degenerate polar phonon modes according to $T_{1u} \rightarrow A_{2u} \oplus E_u$ for AFM-I and $T_{1u} \rightarrow A_2 \oplus E$ for AFM-II. The one-dimensional A_{2u} and A_2 irreducible representations transform as a vector along the z axis, while the two-dimensional E_u and E irreducible representations transform as a vector in the xy plane.

In order to evaluate this splitting we calculated the polar phonons for the AFM-I and AFM-II orderings by diagonalizing the three 5×5 blocks of the dynamical matrix using the T_{1u} symmetry-adapted modes, $f_{n,\alpha}$ [37]. Since we are interested in the splitting generated by the spin pattern alone, similarly as in Ref. [8] we neglected the magnetically induced tetragonal distortion of the crystal and performed calculations for the cubic structure found using FM configuration.

The results are shown in Fig. 4. The phonon frequencies obtained from the $\alpha = x$ and $\alpha = y$ dynamical matrix blocks are equal and form E_u or E doublets. On the other hand, the phonon frequencies obtained from the $\alpha = z$ block are different and correspond to A_{2u} and A_2 singlets. The phonon splitting is the largest for the second lowest frequency mode (except for $MgCr_2O_4$ where it is the lowest frequency mode that has the highest splitting). In particular, for $ZnCr_2O_4$ in AFM-I state it becomes as large as 41 cm^{-1}. Interestingly, the magnitude of the splitting for the AFM-I order is, in general, about twice as large than it is for the AFM-II state.

The most important feature, however, is that for all considered compounds and for all the modes the singlet has a higher energy for the AFM-I state while for the AFM-II configuration it is the doublet that has a higher energy. This is in agreement with the experimentally observed sign reversal of the phonon splitting for $ZnCr_2O_4$ and $MgCr_2O_4$ compared with $CdCr_2O_4$ [10,15–17] since the former ones have a ground state similar to AFM-I [2] while the magnetic ordering of the latter can be approximated by AFM-II [33].

V. SPIN-PHONON COUPLING MODEL

In order to better understand the results of our first principles calculations we employ the spin-phonon coupling model in which the T_{1u} block of the force-constant matrix for an arbitrary magnetic state is given by [11]

$$\tilde{C}_{n\alpha,n'\alpha'} = C^{\mathrm{PM}}_{nn'} + 4\sum_j \frac{\partial^2 J_{ij}}{\partial f_{n\alpha}\partial f_{n'\alpha'}}\langle \mathbf{S}_i \cdot \mathbf{S}_j\rangle \tag{2}$$

Here, $\langle \mathbf{S}_i \cdot \mathbf{S}_j\rangle$ is the spin correlation function that is 1 for the FM ordering and either 1 or -1 for the AFM ordering. $C^{\mathrm{PM}}_{nn'}$ is the force-constants matrix in the PM phase. Note that the latter has a O_h cubic symmetry and thus it doesn't depend on the T_{1u} row indices α and α'.

The above expression can be further simplified by using the symmetry of the magnetic state. In particular, the AFM-I and AFM-II (as well as FM) orderings don't induce couplings between different rows of T_{1u} so the force-constant matrix is diagonal in the row indices: $\tilde{C}_{n\alpha,n'\alpha'} = \tilde{C}_{n\alpha,n'\alpha}\delta_{\alpha,\alpha'} \equiv \tilde{C}_{nn'}(\alpha)$. Consequently, we only need $\partial^2 J_{ij}/\partial f_{n\alpha}\partial f_{n'\alpha}$. Considering only the nn exchange interaction, there are only two types of such derivatives: [11] $J''_{nn'\perp} \equiv \partial^2 J_{ij}/\partial f_{n\alpha}\partial f_{n'\alpha}\ \forall\ \hat{\mathbf{r}}_{ij}\cdot\hat{\alpha} = 0$ and $J''_{nn'\parallel} \equiv \partial^2 J_{ij}/\partial f_{n\alpha}\partial f_{n'\alpha}\ \forall\ \hat{\mathbf{r}}_{ij}\cdot\hat{\alpha} \neq 0$, where $\hat{\mathbf{r}}_{ij}$ is the vector linking nn sites i and j and $\hat{\alpha}$ is the unit vector along the α axis. Therefore, we can write

$$\tilde{C}_{nn'}(\alpha) = C^{\mathrm{PM}}_{nn'} + 4J''_{nn'\perp}\sum_{\hat{\mathbf{r}}_\perp}\langle \mathbf{S}_i \cdot \mathbf{S}_j\rangle + 4J''_{nn'\parallel}\sum_{\hat{\mathbf{r}}_\parallel}\langle \mathbf{S}_i \cdot \mathbf{S}_j\rangle \tag{3}$$

where the first summation is over the two nn in the plane perpendicular to α, and the second summation is over the other four nn. For the three magnetic orderings considered, we obtain

$$\tilde{C}^{\mathrm{FM}}_{nn'}(\alpha = x,y,z) = C^{\mathrm{PM}}_{nn'} + 8J''_{nn'\perp} + 16J''_{nn'\parallel} \tag{4}$$

$$\tilde{C}^{\text{AFM-I}}_{nn'}(\alpha = x,y) = C^{\mathrm{PM}}_{nn'} - 8J''_{nn'\perp} \tag{5}$$

$$\tilde{C}^{\text{AFM-I}}_{nn'}(\alpha = z) = C^{\mathrm{PM}}_{nn'} + 8J''_{nn'\perp} - 16J''_{nn'\parallel} \tag{6}$$

$$\tilde{C}^{\text{AFM-II}}_{nn'}(\alpha = x,y) = C^{\mathrm{PM}}_{nn'} - 8J''_{nn'\parallel} \tag{7}$$

$$\tilde{C}^{\text{AFM-II}}_{nn'}(\alpha = z) = C^{\mathrm{PM}}_{nn'} - 8J''_{nn'\perp} \tag{8}$$

The above equations explicitly demonstrate that in the FM state we have a threefold degeneracy with respect to α and that in the AFM-I and AFM-II states these triplets split into a doublet ($\alpha = x,y$) and a singlet ($\alpha = z$).

The parameters $C^{\mathrm{PM}}_{nn'}$, $J''_{nn'\perp}$, and $J''_{nn'\parallel}$ were fitted to the *ab initio* force-constant matrices evaluated for FM, AFM-I, and AFM-II orderings. Essentially perfect fitting was obtained with the misfit lower than 0.03 meV/Å and corresponding phonon frequencies within 1 cm^{-1} of first principles values (see Supplemental Material [28]). This indicates that the spin-phonon coupling model with only nn exchange coupling provides an excellent description of the effect of magnetic order on phonon frequencies in ACr_2O_4 spinels.

Explicit forms of C^{PM}, $J''_\perp$, and $J''_\parallel$ force-constant matrices for different ACr_2O_4 spinels are shown in the Supplemental Material [28]. We find that for all compounds $J''_{33\perp}$ is positive and significantly larger than any other element of $J''_\perp$ and $J''_\parallel$ matrices. As discussed in Ref. [11], the anomalously large value of $J''_{33\perp}$ originates from the exponential form of the direct exchange contribution (J_d) to J_1. Indeed, $J_d = Ae^{-aD_{\text{Cr-Cr}}}$ where A and a are positive constants and $D_{\text{Cr-Cr}}$ is the nn Cr-Cr bond length. The only partner function that significantly affects $D_{\text{Cr-Cr}}$ is $f_{3\alpha}$ (with $\hat{\alpha}$ perpendicular to the bond) [10] resulting in large $J''_{33\perp}$. This explanation is consistent with the fact that the $J''_{33\perp}$ element is similar for $MgCr_2O_4$ and $ZnCr_2O_4$ compounds but it decreases with the size of A ion due to diminished role of the direct exchange mechanism. Note also that the positive sign of $J''_{33\perp}$ is the direct consequence of the exponential dependence of J_d on the atomic displacements which requires the second derivative to have the same sign as J_d.

The second largest element among $J''_\perp$ and $J''_\parallel$ matrices is $J''_{35\perp}$ (or $J''_{53\perp}$). Since $f_{5\alpha}$ corresponds to the displacement of O sublattice which modifies Cr-O-Cr angle, this shows that the superexchange mechanism also contributes to the spin-phonon coupling. However, the superexchange contribution to the spin-phonon coupling is always significantly smaller than the direct exchange contribution. This remains true even for

$HgCr_2O_4$ compound where the superexchange interaction is stronger than the direct exchange coupling. We believe that this relative ineffectiveness of the superexchange in generating a spin-phonon coupling is a generic feature and is due to the fact that this mechanism doesn't depend so strongly on atomic displacement as the direct exchange mechanism. This feature plays also an important role in the success of our spin-phonon coupling model where we considered only nn exchange interaction. Indeed, while for for $MgCr_2O_4$ and $ZnCr_2O_4$ J_1 is at least an order of magnitude larger than other exchange parameters, in the case of $CdCr_2O_4$ and $HgCr_2O_4$ compounds the J_3 and J_3' couplings are not negligible and our approximation works only because these couplings originates from superexchange processes and have a weak dependence on atomic displacements.

Having established and understood the validity of our spin-phonon coupling we can now use it to provide an additional insight into magnetically induced phonon splitting. Since $J''_{nn'\perp}$ and $J''_{nn'\parallel}$ are much smaller than the elements of the paramagnetic force-constant matrix, the phonon frequencies can be written as

$$\tilde{\omega}_\lambda(\alpha) \approx \omega_\lambda^{\mathrm{PM}} + \frac{2}{\omega_\lambda^{\mathrm{PM}}} \times \left(\mathcal{J}''_{\lambda\perp} \sum_{\hat{\mathbf{r}}_\perp} \langle \mathbf{S}_i \cdot \mathbf{S}_j \rangle + \mathcal{J}''_{\lambda\parallel} \sum_{\hat{\mathbf{r}}_\parallel} \langle \mathbf{S}_i \cdot \mathbf{S}_j \rangle \right) \quad (9)$$

Here, $\omega_\lambda^{\mathrm{PM}}$ is the paramagnetic phonon frequency and for each phonon mode we introduced: $\mathcal{J}''_{\lambda\perp,\parallel} = u_\lambda^\dagger J''_{\perp,\parallel} u_\lambda$ where u_λ are the paramagnetic dynamical matrix eigenvectors and $J''_{\perp,\parallel}$ is the dynamical matrix corresponding to $J''_{nn'\perp,\parallel}$ force-constant matrix. The magnetically-induced phonon splittings for the two principle AFM orders are then given by

$$\begin{aligned} \Delta\omega_\lambda^{\text{AFM-I}} &\equiv \tilde{\omega}_\lambda^{\text{AFM-I}}(\alpha = z) - \tilde{\omega}_\lambda^{\text{AFM-I}}(\alpha = x, y) \\ &\approx 8\mathcal{J}''_{\lambda\perp}/\omega_\lambda^{\mathrm{PM}} - 8\mathcal{J}''_{\lambda\parallel}/\omega_\lambda^{\mathrm{PM}} \end{aligned} \quad (10)$$

$$\begin{aligned} \Delta\omega_\lambda^{\text{AFM-II}} &\equiv \tilde{\omega}_\lambda^{\text{AFM-II}}(\alpha = z) - \tilde{\omega}_\lambda^{\text{AFM-II}}(\alpha = x, y) \\ &\approx -4\mathcal{J}''_{\lambda\perp}/\omega_\lambda^{\mathrm{PM}} + 4\mathcal{J}''_{\lambda\parallel}/\omega_\lambda^{\mathrm{PM}}. \end{aligned} \quad (11)$$

The ratio $\mathcal{J}''_{\lambda\perp,\parallel}/\omega_\lambda^{\mathrm{PM}}$ characterize the strength of the magnetic contribution to the phonon frequencies. Table I shows these parameters for different ACr_2O_4 spinels. We can immediately observe that the only appreciable ratio are $\mathcal{J}''_{\lambda\perp}/\omega_\lambda^{\mathrm{PM}}$ for the two lowest-frequency modes ($\lambda = 1,2$) and both are always positive. It follows from Eqs. (10) and (11) that the phonon splitting is the largest for the two lowest-frequency modes and it is positive (negative) for the AFM-I (AFM-II) orderings. This feature is a direct consequence of $J''_{33\perp}$ being positive and dominant among other elements of $J''_\perp$ and $J''_\parallel$ since the $\lambda = 1,2$ modes have the largest content of the $f_{3\alpha}$ partner function (see Supplemental Material [28]). Therefore, according to the discussion above, different signs of the phonon splittings that we found from first principles for the lowest phonon modes are ultimately related to the dominant role of the direct exchange mechanism in generating the spin-phonon coupling.

Interestingly, $\mathcal{J}''_{\lambda\perp}/\omega_\lambda^{\mathrm{PM}}$ for $\lambda = 3,4$ are also always positive while $\mathcal{J}''_{\lambda\parallel}/\omega_\lambda^{\mathrm{PM}}$ for all modes are consistently negative. This results in the sign of the phonon splitting to be positive (negative) for the AFM-I (AFM-II) states for the two-highest phonon modes as well. These features, however, is difficult to explain microscopically due to small values of the splittings. In fact, the splitting of the two-highest phonon modes is too small to be seen in experiments.

According to Eqs. (10) and (11) we can write

$$\Delta\omega_\lambda^{\text{AFM-II}} \approx -\tfrac{1}{2}\Delta\omega_\lambda^{\text{AFM-I}}. \quad (12)$$

Therefore, the phonon splittings for AFM-I and AFM-II orders are always opposite and the latter is approximately half of the former. This is a general result which follows directly from the applicability of the nn spin-phonon coupling model and it is independent on the signs and sizes of the exchange second derivatives. Note that the above relation is well satisfied by first principles data (Fig. 4) which again demonstrates applicability of the model. Note, however, that this relation doesn't tell us for which ordering the phonon splitting is positive. In order to answer this question more microscopic analysis (as above) is needed.

VI. CONCLUSIONS

In summary, we investigated the effect of magnetic ordering on phonon frequencies of ACr_2O_4 spinels using first principles electronic structure calculations. We found that our *ab initio* results are very well described by the spin-phonon coupling model with only nn exchange coupling [11]. Both the model and first principles calculations show that a specific type of spin ordering has a crucial effect on magnetically induced phonon splitting. In particular, we found that the different magnetic states observed in different spinels lead to the opposite signs of the phonon splittings observed in $ZnCr_2O_4$ and $MgCr_2O_4$ compounds compared to $CdCr_2O_4$. This feature is a result of an important role played by the direct exchange mechanism in generating the spin-phonon coupling in these materials.

ACKNOWLEDGMENTS

We acknowledge fruitful discussions with Craig J. Fennie and Karin Rabe. Work at Ames Lab was supported by the U.S. Department of Energy (DOE), Office of Science, Basic Energy Sciences, Materials Science and Engineering Division. Ames Laboratory is operated for the U.S. DOE by Iowa State University under Contract No. DE-AC02-07CH11358. T.B. was supported by the Rutgers Center for Materials Theory.

[1] Y. Yamashita and K. Ueda, Phys. Rev. Lett. **85**, 4960 (2000).

[2] O. Tchernyshyov, R. Moessner, and S. L. Sondhi, Phys. Rev. Lett. **88**, 067203 (2002).

[3] T. Kimura, S. Kawamoto, I. Yamada, M. Azuma, M. Takano, and Y. Tokura, Phys. Rev. B **67**, 180401 (2003).
[4] M. Fiebig, J. Phys. D **38**, R123 (2005).
[5] T. Birol, N. A. Benedek, H. Das, A. L. Wysocki, A. T. Mulder, B. M. Abbett, E. H. Smith, S. Ghosh, and C. J. Fennie, Curr. Opin. Solid State Mater. Sci. **16**, 227 (2012).
[6] G. Lawes, T. Kimura, C. Varma, M. Subramanian, N. Rogado, R. Cava, and A. Ramirez, Prog. Solid State Chem. **37**, 40 (2009).
[7] T. Birol and C. J. Fennie, Phys. Rev. B **88**, 094103 (2013).
[8] S. Massidda, M. Posternak, A. Baldereschi, and R. Resta, Phys. Rev. Lett. **82**, 430 (1999).
[9] W. Luo, P. Zhang, and M. L. Cohen, Solid State Commun. **142**, 504 (2007).
[10] A. B. Sushkov, O. Tchernyshyov, W. Ratcliff, II, S. W. Cheong, and H. D. Drew, Phys. Rev. Lett. **94**, 137202 (2005).
[11] C. J. Fennie and K. M. Rabe, Phys. Rev. Lett. **96**, 205505 (2006).
[12] K. T. Chan, J. D. Sau, P. Zhang, and M. L. Cohen, Phys. Rev. B **75**, 054304 (2007).
[13] W. Baltensperger and K. S. Helman, Helv. Phys. Acta **41**, 668 (1968).
[14] W. Baltensperger, J. Appl. Phys. **41**, 1052 (1970).
[15] R. Valdés Aguilar, A. B. Sushkov, Y. J. Choi, S.-W. Cheong, and H. D. Drew, Phys. Rev. B **77**, 092412 (2008).
[16] C. Kant, J. Deisenhofer, T. Rudolf, F. Mayr, F. Schrettle, A. Loidl, V. Gnezdilov, D. Wulferding, P. Lemmens, and V. Tsurkan, Phys. Rev. B **80**, 214417 (2009).
[17] C. Kant, M. Schmidt, Z. Wang, F. Mayr, V. Tsurkan, J. Deisenhofer, and A. Loidl, Phys. Rev. Lett. **108**, 177203 (2012).
[18] J. H. Lee and K. M. Rabe, Phys. Rev. B **84**, 104440 (2011).
[19] A. Kumar, C. J. Fennie, and K. M. Rabe, Phys. Rev. B **86**, 184429 (2012).
[20] Y. Zhou and K. M. Rabe, Phys. Rev. B **88**, 094416 (2013).
[21] T. Shen, K. Cao, G.-C. Guo, and L. He, Phys. Rev. B **78**, 134413 (2008).
[22] A. I. Liechtenstein, V. I. Anisimov, and J. Zaanen, Phys. Rev. B **52**, R5467 (1995).
[23] J. P. Perdew, A. Ruzsinszky, G. I. Csonka, O. A. Vydrov, G. E. Scuseria, L. A. Constantin, X. Zhou, and K. Burke, Phys. Rev. Lett. **100**, 136406 (2008).
[24] C. J. Fennie and K. M. Rabe, Phys. Rev. B **72**, 214123 (2005).
[25] P. E. Blöchl, Phys. Rev. B **50**, 17953 (1994).
[26] G. Kresse and J. Hafner, Phys. Rev. B **48**, 13115 (1993).
[27] G. Kresse and J. Furthmüller, Phys. Rev. B **54**, 11169 (1996).
[28] See Supplemental Material at http://link.aps.org/supplemental/10.1103/PhysRevB.93.134425 for structural data, the details of the symmetry adapted modes, and fitting results.
[29] H. T. Stokes, D. M. Hatch, and B. J. Campbell, ISOTROPY, http://stokes.byu.edu/isotropy.html (2007).
[30] A. N. Yaresko, Phys. Rev. B **77**, 115106 (2008).
[31] J. B. Goodenough, J. Phys. Chem. Solids **30**, 261 (1969).
[32] K. Dwight and N. Menyuk, Phys. Rev. **163**, 435 (1967).
[33] G.-W. Chern, R. Moessner, and O. Tchernyshyov, Phys. Rev. B **78**, 144418 (2008).
[34] G.-W. Chern, C. J. Fennie, and O. Tchernyshyov, Phys. Rev. B **74**, 060405 (2006).
[35] H. J. Xiang, E. J. Kan, S.-H. Wei, M.-H. Whangbo, and X. G. Gong, Phys. Rev. B **84**, 224429 (2011).
[36] M. Matsuda, H. Ueda, A. Kikkawa, Y. Tanaka, K. Katsumata, Y. Narumi, T. Inami, Y. Ueda, and S.-H. Lee, Nat. Phys. **3**, 397 (2007).
[37] Under D_{4h} or D_4 certain rows of the silent T_{2u} irreducible representation of O_h become ir-active and can in principle mix with the irreducible representations originating from T_{1u}. This mixing is small, however, (as we explicitly checked) and therefore was neglected.